INT. J. NUM. METH. HEAT FLUID FLOW, VOL. 4, 465–476 (1994)

NATURAL CONVECTION HEAT TRANSFER AROUND TWO HEATED CYLINDERS IN AN ISOTHERMAL ENCLOSURE INCLUDING THE EFFECT OF WALL CONDUCTANCE

MARCEL LACROIX AND ANTOINE JOYEUX

Département de Génie Mécanique, Université de Sherbrooke, Sherbrooke, Québec, J1K 2R1, Canada

ABSTRACT

A numerical study has been conducted for natural convection heat transfer for air around two vertically separated horizontal heated cylinders placed inside an isothermal rectangular enclosure having finite wall conductances. The interaction between convection in the fluid filled cavity and conduction in the walls surrounding the cavity is investigated. Results have been obtained for Rayleigh numbers (Ra) between 10^3 and 10^6, dimensionless wall thickness ($\bar{W}$) between 0.5 and 1.375 and dimensionless wall-fluid thermal conductivity ratio ($\bar{\alpha}$) between 0.01 and 5.0. The results indicate that wall heat conduction reduces the average temperature differences across the cavity, partially stabilizes the flow, and decreases natural convection heat transfer. The overall heat transfer coefficient for both cylinders is correlated with CRa^n for different $\bar{W}$ and $\bar{\alpha}$.

KEY WORDS Wall heat conductance Natural convection Circular cylinders

NOMENCLATURE

D	diameter of cylinders,
g	acceleration of gravity,
H	cavity height,
$\bar{H}$	dimensionless height ($= H/D$)
$\underline{H1}$	vertical height of cylinder no. 1,
$H1$	dimensionless height ($= H1/D$),
$\underline{H2}$	vertical height of cylinder no. 2,
$H2$	dimensionless height ($= H2/D$),
J	Jacobian,
k	thermal conductivity,
L	half width of cavity,
$\bar{L}$	dimensionless width ($= L/D$),
$\underline{Nu}$	local Nusselt number,
$\overline{Nu}$	average Nusselt number,
Nu_0	overall Nusselt number,
Pr	Prandtl number (ν_f/α_f),
Ra	Rayleigh number ($g\beta(T_H - T_C)D^3/\nu_f\alpha_f$),
$S(x, y)$	source term,
T_C	temperature of outside surfaces of walls,
T_H	temperature of heated cylinders,
u	dimensionless velocity in the x direction (u^*D/α_f),
v	dimensionless velocity in the y direction (v^*D/α_f),
U	geometric coefficient,
V	geometric coefficient,
W	wall thickness,
$\bar{W}$	dimensionless thickness ($= w/D$),
x	dimensionless coordinate ($x = x^*/D$),
y	dimensionless coordinate ($y = y^*/D$),
α	thermal diffusivity and geometric coefficient,
$\bar{\alpha}$	dimensionless conductivity ratio ($= k_w/k_f$),
β	thermal expansion coefficient and geometric coefficient,
γ	geometric coefficient,
Γ	exchange coefficient,

0961–5539/94/040465–12$2.00

Received August 1993
Revised January 1994

η transformed coordinate,
θ dimensionless temperature $\left(\theta = \frac{T - T_C}{T_H - T_C}\right)$,
ν kinematic viscosity,
ξ transformed coordinate,
ρ constant,
ϕ general dependent variable,
ψ dimensionless stream function,
ω dimensionless vorticity,

Superscripts

* indicates a dimensional quantity,

Subscripts

C cooled surface,
f fluid,
H heated surface,
w wall.

SW, S, SE, etc. South West, South, South East, etc. (equation 7)

INTRODUCTION

Natural convection heat transfer around horizontal circular cylinders finds numerous practical applications in space heating, heat exchangers, solar energy collectors, energy storage systems, and electronic devices. As a result, the subject has been of considerable research interest.

Several studies have been conducted to investigate natural convection heat transfer from horizontal cylinders in free space[1–4] or bounded by parallel plates[5–7]. However, comparatively little numerical work on free convective heat transfer from circular cylinders confined to an enclosure has been reported. Perhaps, it is due to the challenging task of simulating the strong interaction between the boundary layer and the adjacent fluid in a geometrically complicated enclosure.

Recently, numerical studies of natural convection heat transfer around two horizontal heated cylinders confined to a rectangular enclosure have been reported by one of the authors[8,9]. The effect of the boundary conditions and of the geometric configuration on the heat transfer was investigated. These studies neglected, however, the interaction between convection in the fluid filled cavity and conduction in the walls surrounding the cavity. Idealized boundary conditions corresponding to prescribed temperatures at the cooled wall and perfectly conducting walls at adiabatic walls were used. In spite of the fact that these boundary conditions were completely justified, there are some physical situations where heat conduction in the material forming the enclosure walls must also be considered. An example of such a situation includes circular pipes inside walls for space heating. Other examples are reported in the excellent studies of Kim and Viskanta[10] and Du and Bilgen[11] on conjugate heat transfer in a rectangular enclosure.

The intent of this paper is to investigate numerically natural convection heat transfer from a pair of vertically separated horizontal heated cylinders confined to a rectangular enclosure formed by finite conductance walls. A mathematical model is formulated and a numerical procedure is developed to solve the model equations. Parametric studies are then conducted to examine the effect of the Rayleigh number, of the wall thickness and of the thermal conductivity ratio on the fluid flow and heat transfer inside the cavity.

PHYSICAL MODEL AND NUMERICAL PROCEDURE

The physical model of the problem is illustrated schematically in *Figure 1*. A two-dimensional cavity of height H and of width $2L$ is formed by walls of uniform thickness W and of thermal conductivity k_w. The enclosure contains two horizontal circular cylinders situated one above the other in the vertical centre-axis. The diameter D of the cylinders serves as the characteristic length scale on which the Rayleigh number is based. The lower and upper cylinders are located at a distance $H1$ and $H2$ respectively from the bottom of the cavity. The outside surface of the

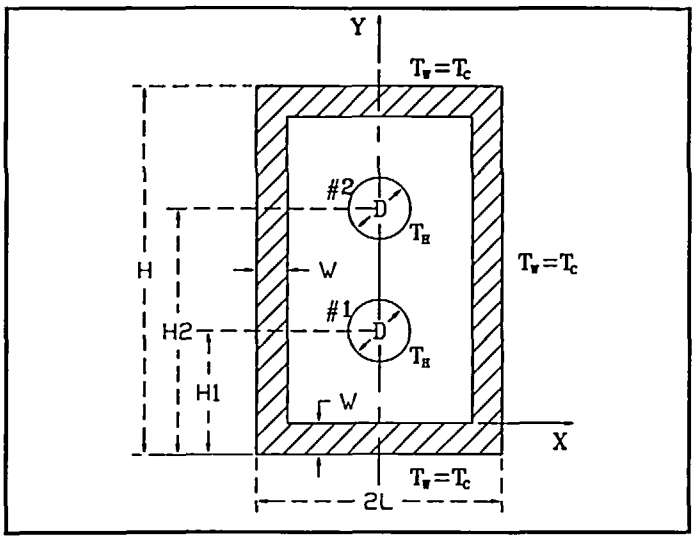

Figure 1 Schematic representation of the enclosure with horizontal cylinders

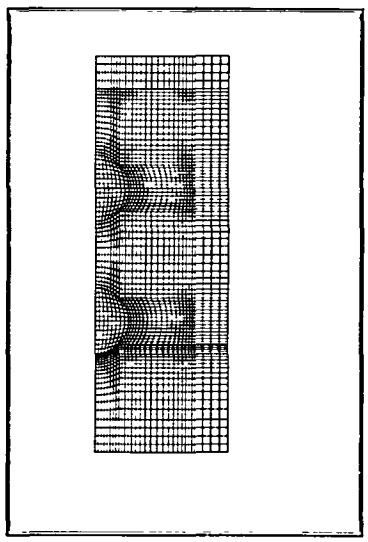

Figure 2 Transfinite interpolated curvilinear grid (31 × 83 nodes)

walls is maintained at a constant temperature T_C while the cylinders surface is kept a constant temperature T_H ($T_H > T_C$).

It is assumed in the analysis that the thermophysical properties of the walls and of the fluid are independent of temperature, and the flow is laminar. The fluid is Newtonian, incompressible, and the Boussinesq approximation is valid. The fluid motion and heat transfer in the cavity are assumed to be two-dimensional and symmetrical about the vertical centreline. Radiation is neglected in comparison to convection.

With the foregoing assumptions, the governing partial differential equations in dimensionless form for the conservation of mass, momentum, and energy are cast in terms of vorticity, stream function, and temperature. Moreover, to deal effectively with the geometrical complicated solution domain of the present problem, a curvilinear grid, as exemplified in *Figure 2*, is employed. Based on this boundary-fitted coordinate grid, the conservation equations and their boundary conditions are cast from the original cartesian reference frame (x, y) to a generalized curvilinear grid (ξ, η). The resulting transport equations in the transformed plane are more complicated but the boundary conditions are now specified on straight boundaries and the computational grid is rectangular and uniformly spaced. Performing this transformation[8], the general transport equation for the flow property ϕ takes the following form in the computational space (ξ, η):

$$\frac{1}{J}\frac{\partial}{\partial \xi}\left[(\rho U\phi) - \frac{\Gamma}{J}\left(\alpha\frac{\partial \phi}{\partial \xi} - \beta\frac{\partial \phi}{\partial \eta}\right)\right] + \frac{1}{J}\frac{\partial}{\partial \eta}\left[(\rho V\phi) - \frac{\Gamma}{J}\left(\gamma\frac{\partial \phi}{\partial \eta} - \beta\frac{\partial \phi}{\partial \xi}\right)\right] = S(\xi, \eta) \qquad (1)$$

$S(\xi, \eta)$ is a source term, Γ is an exchange coefficient, and ρ is a constant. These variables and parameters are defined in *Table 1*. The geometric factors U, V, α, β, γ and the Jacobian J are defined as usual as:

$$\begin{aligned} U &= \frac{\partial \psi}{\partial \eta} \\ V &= -\frac{\partial \psi}{\partial \xi} \\ \alpha &= \left(\frac{\partial x}{\partial \eta}\right)^2 + \left(\frac{\partial y}{\partial \eta}\right)^2 \\ \beta &= \frac{\partial x}{\partial \xi}\frac{\partial x}{\partial \eta} + \frac{\partial y}{\partial \xi}\frac{\partial y}{\partial \eta} \\ \gamma &= \left(\frac{\partial x}{\partial \xi}\right)^2 + \left(\frac{\partial y}{\partial \xi}\right)^2 \\ J &= \frac{\partial x}{\partial \xi}\frac{\partial y}{\partial \eta} - \frac{\partial x}{\partial \eta}\frac{\partial y}{\partial \xi} \end{aligned} \qquad (2)$$

The stream function is set equal to zero around both cylinders, along the wall-fluid interfaces and along the vertical centreline. The vorticity boundary condition on solid walls is given by:

$$\omega_i = -\frac{2\psi_{i+1}}{\Delta r^2} \qquad (3)$$

where Δr is the distance between a boundary grid node i and the nearest node $i + 1$ inside the fluid. On the vertical symmetry line, $\omega = 0$.

A uniform temperature $\theta_f = 1$ is imposed at the surface of both cylinders while the outside surfaces of the enclosure are maintained at a constant temperature $\theta_w = 0$. The Neumann

Table 1 Variables and parameters of governing transport equation (1)

Function	ϕ	ρ	Γ	$S(\xi, \eta)$
Temperature (wall)	θ_w	1	$\tilde{\alpha}$	0
Temperature (fluid)	θ_f	1	1	0
Vorticity	ω	1	Pr	$\frac{Ra \cdot Pr}{J}\left(\frac{\partial y}{\partial \eta}\frac{\partial \theta_f}{\partial \xi} - \frac{\partial y}{\partial \xi}\frac{\partial \theta_f}{\partial \eta}\right)$
Stream function	ψ	0	1	ω

boundary conditions for the temperature are, at the horizontal wall–fluid interfaces,

$$\frac{\partial \theta_f}{\partial \eta} = \bar{\alpha} \frac{\partial \theta_w}{\partial \eta} \tag{4}$$

at the vertical wall–fluid interface,

$$\frac{\partial \theta_f}{\partial \xi} = \bar{\alpha} \frac{\partial \theta_w}{\partial \xi} \tag{5}$$

and, at the vertical symmetry line,

$$\frac{\partial \theta_w}{\partial \xi} = \frac{\partial \theta_f}{\partial \xi} = 0 \tag{6}$$

The finite difference equations are obtained on integrating the general governing equation (1), over each of the control volumes in the (ξ, η) plane. The resulting finite difference scheme has the form:

$$\mathrm{ASW}\cdot\phi_{\mathrm{SW}} + \mathrm{AS}\cdot\phi_{\mathrm{S}} + \mathrm{ASE}\cdot\phi_{\mathrm{SE}} + \mathrm{AW}\cdot\phi_{\mathrm{W}} + \mathrm{AP}\cdot\phi_{\mathrm{P}} + \mathrm{AE}\cdot\phi_{\mathrm{E}} + \mathrm{ANW}\cdot\phi_{\mathrm{NW}} + \mathrm{AN}\cdot\phi_{\mathrm{N}} + \mathrm{ANE}\cdot\phi_{\mathrm{NE}} = Q \tag{7}$$

Expressions for the coefficients in (7) may be found in Reference 12. The terms arising from the non-orthogonality of the grid appear in the coefficients of the crossed terms ASW, ASE, ANW, and ANE. Q is the discretized source term S. The advection-diffusion part of coefficients AS, AW, AP, AE, and AN is modified for stability according to the power-law scheme of Patankar[13].

Equation (7) is solved iteratively for θ, ω and ψ using an alternating line by line solver. The temperature equation is solved for the walls and the fluid simultaneously by setting $u = v = 0$ across the walls. Convergence is declared when the largest residual for all difference equations is smaller than 10^{-3}. More stringent convergence criteria were retained but the results did not show noticeable changes in the final solutions.

The foregoing computational model was thoroughly tested for natural convection heat transfer inside enclosures with irregular boundaries and for different flow conditions. Its accuracy was also checked by comparison with experimental data for natural convection heat transfer from heated protrusions on a vertical wall in a rectangular cavity. These validation analyses are reported in References 8, 9 and 12 and need not be repeated here.

RESULTS AND DISCUSSION

There are a large number of independent parameters ($\overline{H1}$, $\overline{H2}$, $\bar{H}$, $\bar{L}$, $\bar{W}$, Ra, Pr and $\bar{\alpha}$) governing the problem, and it is not feasible to obtain solutions for the complete range of interest. Extensive numerical experiments were, however, conducted for combined conduction and laminar natural convection around horizontal circular cylinders of fixed position, i.e. $\overline{H1} = 2.0$ and $\overline{H2} = 4.0$ confined to a rectangular enclosure of height $\bar{H} = 6.0$ and width $2\bar{L} = 4.0$. The wall thickness $\bar{W}$ ranged from 0.5 to 1.375 and its thermal conductivity ratio $\bar{\alpha}$ ranged from 0.01 to 5.0. Obviously, as $\bar{W}$ increases, the available space for the fluid confined to the fixed cavity size diminishes. Due to the possible applications that motivated this analysis, the Prandtl number (Pr) was set to a constant value for air ($Pr = 0.71$) and the Rayleigh number (Ra) ranged from 10^3 to 10^6.

The accuracy of the present calculation has been investigated by performing a grid refinement study. As a result, simulations reported here were conducted with grid sizes ranging from 31 × 83 to 35 × 91 non-uniformly distributed nodes. Results obtained with finer meshes did not show noticeable changes in the predicted flow fields and in the local heat transfer coefficients.

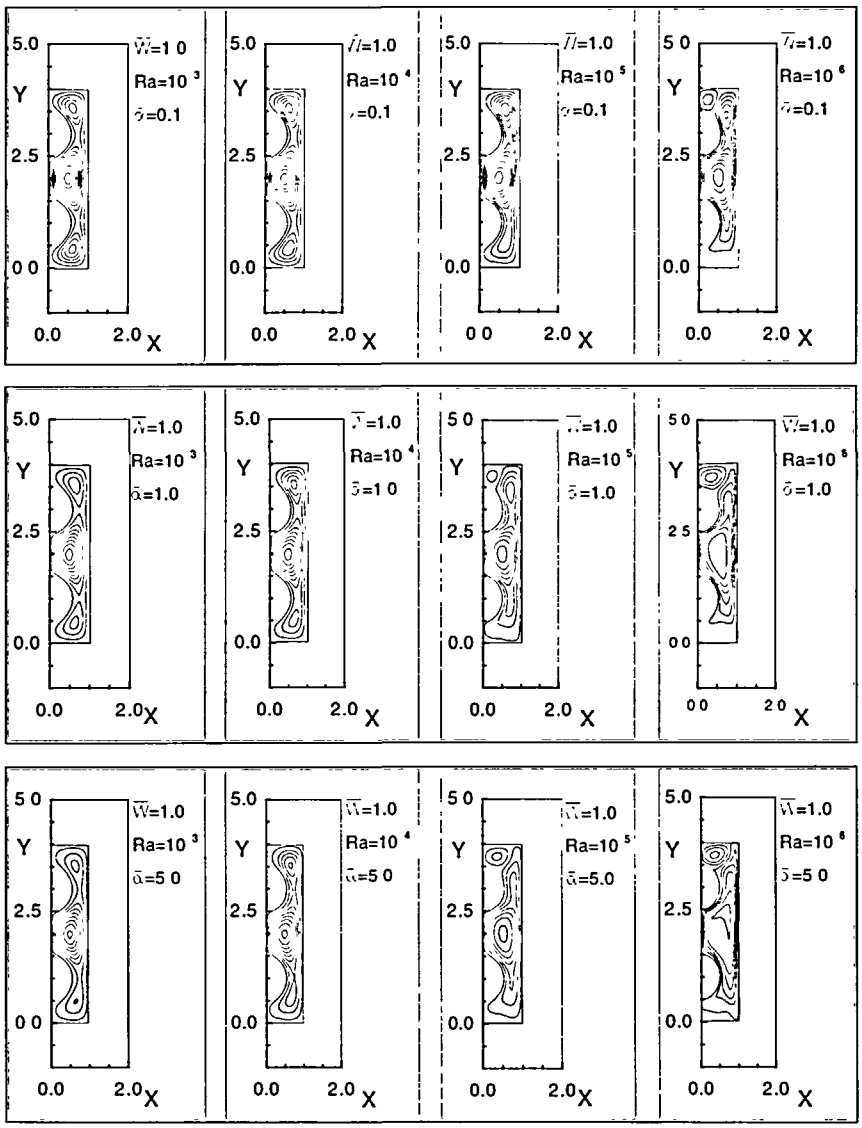

Figure 3 Predicted streamlines for $\bar{W} = 1.0$, $0.1 \leqslant \bar{\alpha} \leqslant 5.0$ and $10^3 \leqslant Ra \leqslant 10^6$

As an example, *Figures 3* and *4* illustrate the contours of the streamlines and of the isotherms for few cases studied with a wall of thickness $\bar{W} = 1.0$. For both Figures, the thermal conductivity ratio $\bar{\alpha}$ increases from the top to the bottom of the picture and the Rayleigh number (Ra) increases from the left to the right. In the present study, the Rayleigh number is based on the overall temperature difference $T_H - T_C$. In the cases for which $\bar{\alpha}$ is small ($\bar{\alpha} \leqslant 0.1$), the effective Rayleigh number in the air is, however, very low and, as a result, the convective motion is very weak. *Figures 3* and *4* clearly show that the buoyancy driven circulation intensifies as $\bar{\alpha}$ and/or Ra increase in magnitude. For small thermal conductivity ratios, i.e. $\bar{\alpha} \leqslant 1.0$ and, in general, for low and intermediate Rayleigh numbers, it is seen that three independent recirculating bubbles

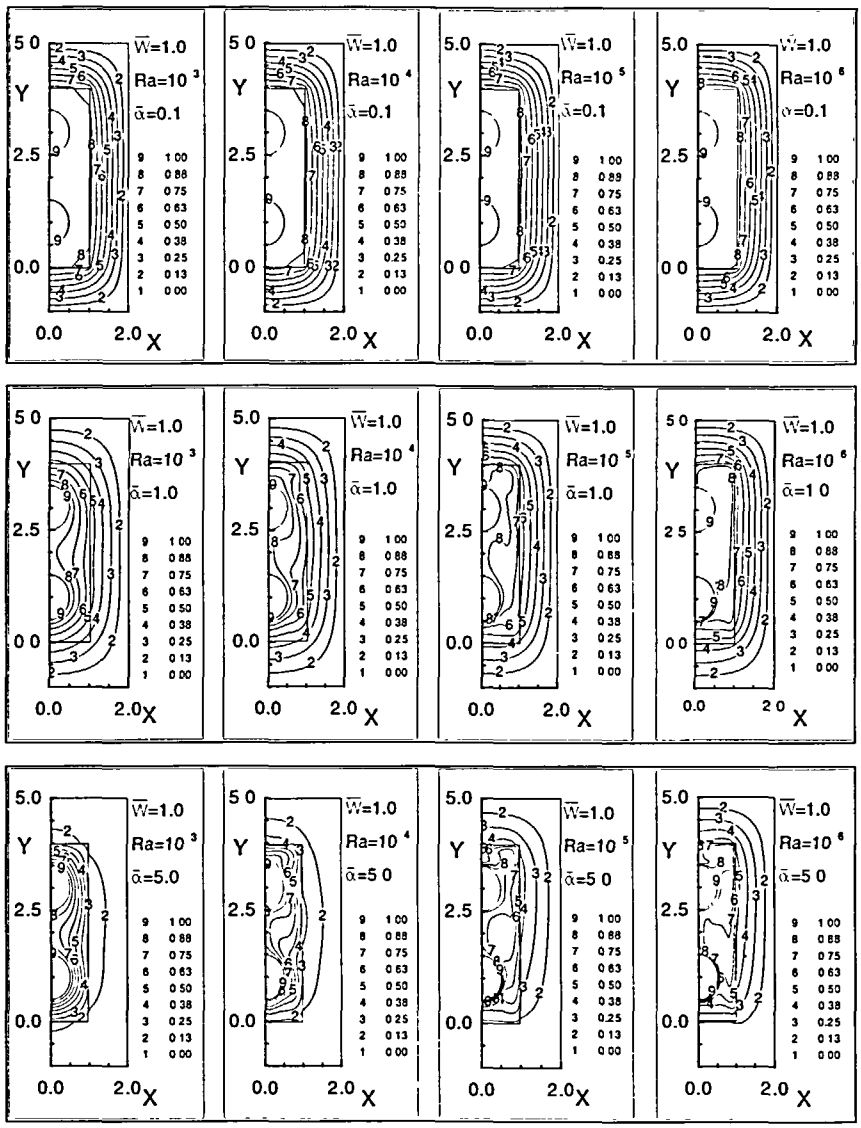

Figure 4 Predicted isotherms for $\bar{W} = 1.0$, $0.1 \leqslant \bar{\alpha} \leqslant 5.0$ and $10^3 \leqslant Ra \leqslant 10^6$

prevail in the cavity: one small eddy at the bottom of the cavity, one between both cylinders and one at the top. As $\bar{\alpha}$ and Ra increase (it becomes evident for $\bar{\alpha} \geqslant 1.0$ and $Ra \geqslant 10^5$), the recirculating eddy in the middle of the cavity stretches and eventually engulfs the recirculating eddy at the bottom. At the same time, a small counterclockwise recirculating eddy appears above the top cylinder. This flow behaviour, as it will be seen later, strongly affects heat transfer around the top cylinder and along the top horizontal wall-fluid interface. For $\bar{\alpha} \leqslant 0.1$, the flow remains nearly stagnant as the effective Rayleigh number is small. The thermal resistance across the cavity walls is significant as shown by the temperature gradients in *Figure 4*. Consequently, the temperature distribution inside the fluid filled cavity is nearly uniform. For $\bar{\alpha} \geqslant 1.0$, the

change in the thermal behaviour of the cavity is noticeable. The thermal resistance across the walls becomes smaller than that of the fluid filled cavity and the temperature gradients across the fluid layer are considerably perturbed by the stronger buoyancy driven flows. On the other hand, as the Rayleigh number increases in magnitude, the thermal resistance across the fluid filled cavity becomes smaller and the temperature drop through the cavity wall increases. This behaviour is clearly illustrated by the second row in *Figure 4* for which $\bar{\alpha} = 1.0$. For $Ra = 10^3$, the flow is nearly stagnant. Conduction is the prevailing mode of heat transfer inside the fluid and the isotherms remain equidistant and parallel to the cooled horizontal and vertical walls. The thermal resistance across the fluid filled cavity is nearly the same as that of the walls. As the Rayleigh number increases, however, buoyancy driven convection inside the fluid prevails increasingly over conduction thus reducing the resistance to heat flow across the fluid layer. Consequently, the thermal resistance across the cavity is now ruled by the conduction resistance through the walls.

Similar numerical experiments were carried out for different wall thickness, i.e. $\bar{W} = 0.5$, 1.25 and 1.375. For $\bar{W} = 0.5$, the cavity space for the fluid is larger and as a result, the middle recirculation eddy engulfs the bottom recirculation bubble for values of $\bar{\alpha}$ and Ra smaller in magnitude than those for the corresponding cases with $\bar{W} = 1.0$. Furthermore, for $\bar{\alpha} \geqslant 1.0$ and high Rayleigh numbers, only one large recirculation eddy prevails in the entire cavity. The secondary counterclockwise eddy at the top of the cavity for $\bar{\alpha} \geqslant 1.0$ and $Ra \geqslant 10^5$ (*Figure 3*) is not observed. On the other hand, for the cases with the smallest fluid filled cavity spaces, i.e. $\bar{W} \geqslant 1.25$, the three recirculation eddies (top, middle and bottom) never merge even for $\bar{\alpha} = 5.0$ and $Ra = 10^6$ as the gaps between the cylinders and the vertical wall–fluid interface are too narrow ($= 0.125$).

Due to the limited space, the results for the streamlines and isotherms for $\bar{W} = 0.5$, 1.25 and 1.375 are not shown here. However, the main conclusion that can be drawn from these experiments is that the fluid space clearly affects the natural convection flow patterns and therefore the heat transfer rates around the cylinder surfaces and along the wall–fluid interfaces.

The local Nusselt numbers around the top and the bottom cylinder for $\bar{\alpha} = 1.0$ and $\bar{\alpha} = 5.0$ are depicted in *Figures 5a* and *5b*, respectively. The local Nusselt number is defined as: $Nu = -\partial\theta_f/\partial n$ where n is a normal coordinate to the cylinder surface. The angle, in degrees, is measured counterclockwise from the bottom of the cylinder. In both cases, the heat transfer coefficient is, as expected, larger for larger thermal conductivity ratios and increasing Rayleigh numbers. The Nusselt number has a maximum value underneath the bottom cylinder (0 degrees) and decreases steadily as the angle increases. For the top cylinder and when natural convection heat transfer prevails, i.e. $Ra \geqslant 10^5$, two maxima are observed. A first maximum is reached underneath the top cylinder (0 degrees) where cold fluid is brought by the large clockwise recirculating eddy. A second maximum is reached on top of the upper cylinder (180 degrees) where cold fluid from the small counterclockwise recirculation bubble impinges on its surface.

Figure 6 illustrates the variation of the average Nusselt number around each cylinder as a function of the Rayleigh number and for different thermal conductivity ratios and wall thicknesses.

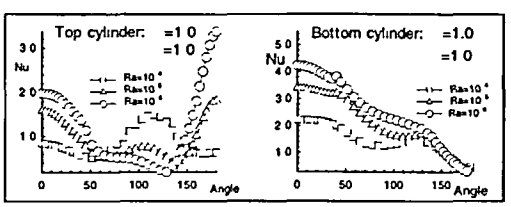

Figure 5a Local Nusselt number around top and bottom cylinders; $\bar{W} = 1.0$ and $\bar{\alpha} = 1.0$

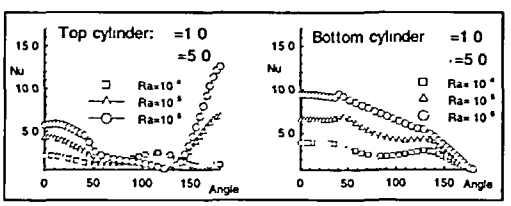

Figure 5b Local Nusselt number around top and bottom cylinders; $\bar{W} = 1.0$ and $\bar{\alpha} = 5.0$

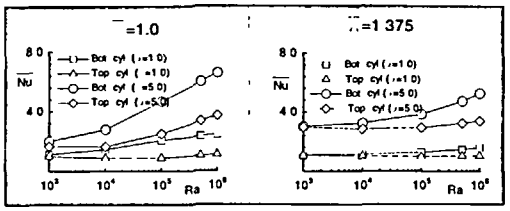

Figure 6 Average Nusselt number for both cylinders; $\bar{W} = 1.0$ and 1.375; $\bar{\alpha} = 1.0$ and 5.0

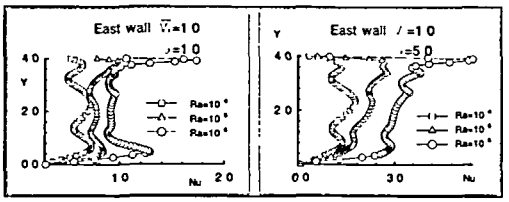

Figure 7 Local Nusselt number along the vertical wall-fluid interface; $\bar{W} = 1.0$, $\bar{\alpha} = 1.0$ and 5.0

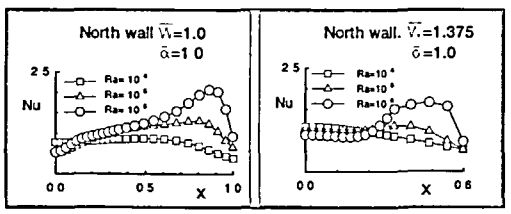

Figure 8 Local Nusselt number along the top horizontal wall-fluid interface; $\bar{\alpha} = 1.0$, $\bar{W} = 1.0$ and 1.375

The average Nusselt number $\overline{Nu}$ at the cylinder surface is given by:

$$\overline{Nu} = -\frac{1}{\pi}\int_0^{\pi} \frac{\partial \theta_f}{\partial n}\, d\sigma$$

For all cases, the cooling rate around the bottom cylinder remains higher than that for the top cylinder as the latter is poorly cooled by the hot fluid rising from the former. This difference in the average Nusselt numbers increases as the buoyancy driven convection intensifies. On the other hand, when $\bar{\alpha}$ diminishes, conduction heat transfer inside the fluid filled cavity plays an increasingly important role compared to convection heat transfer and the cooling rates around both cylinders become closer. Moreover, increasing the wall thickness $\bar{W}$ decreases the available space for the fluid and increases the wall thermal resistance. Consequently, the buoyancy driven motion is diminished and the resulting heat transfer rates are reduced.

Figure 7 displays the local Nusselt number profile at the vertical wall–fluid interface. As expected, for convection dominated heat transfer ($Ra \geqslant 10^5$), maximum heat transfer is reached at the top of the wall where warm fluid impinges after being heated by both cylinders. As the fluid descends along the wall, heat is transferred to it, the liquid cools and Nu decreases. At the bottom of the interface, $Y = 0$, Nu is null as the isotherms become perpendicular to the vertical wall (*Figure 4*).

The local Nusselt numbers along the top horizontal wall–fluid interface are shown in *Figure 8* for $\bar{W} = 1.0$ and $\bar{W} = 1.375$. For $Ra \leqslant 10^4$, the local Nusselt number is nearly uniform left of the midpoint and then decreases steadily beyond it. For $Ra \geqslant 10^5$, the heat transfer coefficient increases rapidly along the top horizontal wall and reaches a maximum near the corner of the fluid filled cavity. This is caused by the presence of the small counterclockwise recirculating eddy which forces cold fluid to impinge on the top wall. As Ra increases from 10^5 to 10^6, the top recirculation bubble increases in size and pushes the location of the maximum heat transfer further to the right. Once again, a thicker wall dampens the buoyancy driven motion and diminishes the local Nusselt number along the top wall.

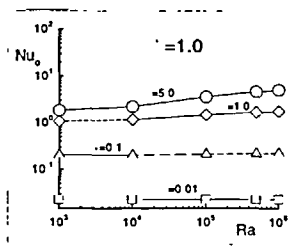

Figure 9 Predicted overall Nusselt number *versus* Rayleigh number for $\bar{W} = 1.0$

Table 2 Overall Nusselt number $\overline{Nu_0}$

	Ra			
$\bar{W}$	10^4	10^5	5×10^5	10^6
		$\bar{\alpha} = 0.1$		
0.5	0.428	0.468	0.495	0.503
1.0	0.204	0.211	0.220	0.225
1.25	0.156	0.157	0.161	0.164
1.375	0.138	0.138	0.140	0.143
		$\bar{\alpha} = 1.0$		
0.5	1.821	2.506	2.934	3.039
1.0	1.173	1.465	1.687	1.780
1.25	1.085	1.193	1.434	1.334
1.375	1.081	1.123	1.238	1.307
		$\bar{\alpha} = 5.0$		
0.5	2.765	4.660	6.186	6.874
1.0	2.224	3.574	4.669	5.128
1.25	2.529	3.131	4.534	4.043
1.375	3.050	3.391	3.985	4.330

The results for the overall Nusselt numbers $\overline{Nu_0}$ around both cylinders have been calculated over a range of Rayleigh numbers, wall thicknesses and thermal conductivity ratios. The overall Nusselt number is defined here as:

$$\overline{Nu_0} = (\overline{Nu_1} + \overline{Nu_2})/2$$

where $\overline{Nu_1}$ and $\overline{Nu_2}$ are the average Nusselt numbers for the top and bottom cylinders respectively. As an example, *Figure 9* displays the variation of $\overline{Nu_0}$ with Ra for different $\bar{\alpha}$. The overall Nusselt numbers for $10^4 \leqslant Ra \leqslant 10^6$, $0.1 \leqslant \bar{\alpha} \leqslant 5.0$ and $0.5 \leqslant \bar{W} \leqslant 1.375$ are summarized in *Table 2*. Scrutiny of *Figure 9* reveals that for convection dominated heat transfer $\overline{Nu_0}$ varies logarithmically with Ra and the slope increases with $\bar{\alpha}$. These results were correlated for $10^4 \leqslant Ra \leqslant 10^6$ with a least squares fit by the following equation

$$\overline{Nu_0} = CRa^n \tag{8}$$

C and n are constants which depend on the wall thickness $\bar{W}$ and on the thermal conductivity ratio $\bar{\alpha}$. Their values are listed in *Table 3*. These results clearly show that the overall Nusselt numbers are more sensitive to the thermal conductivity ratio than to the wall thickness. Obviously, as $\bar{\alpha}$ decreases and/or $\bar{W}$ increases, $\overline{Nu_0}$ decreases.

Table 3 Constants C and n in correlation (8)

$\bar{W}$	$\bar{\alpha}$	C	n
0.5	0.1	0.3084	0.0359
—	1.0	0.6559	0.1132
—	5.0	0.4537	0.1986
1.0	0.1	0.1667	0.0213
—	1.0	0.5100	0.0910
—	5.0	0.4212	0.1830
1.25	0.1	0.1405	0.0107
—	1.0	0.6513	0.0550
—	5.0	0.8272	0.1204
1.375	0.1	0.1295	0.0064
—	1.0	0.7293	0.0406
—	5.0	1.4894	0.0754

CONCLUSION

A numerical study was conducted for natural convection heat transfer around two horizontal heated cylinders confined to an isothermal enclosure having finite wall conductances. The interaction between convection in the fluid filled cavity and conduction in the walls surrounding the cavity was investigated for a wide range of thermal conductivity ratios, fluid spaces and Rayleigh numbers. The results showed the relative importance of the Rayleigh number and of the thermal conductivity ratio on the thermal behaviour of the cavity. Heat conduction in the walls not only reduces the average temperature difference across the cavity but also produces partial stabilization of the flow and decreases natural convection heat transfer. The overall Nusselt number was correlated with CRa^n.

ACKNOWLEDGEMENTS

The authors gratefully acknowledge the financial support of the Natural Sciences and Engineering Research Council of Canada and of the Ministère de l'énergie et des resources du Québec. They also thank Miss Plante for typing this manuscript.

REFERENCES

1 Kuehn, T. H. and Goldstein, R. J. Numerical solution to the Navier–Stokes equations for laminar natural convection about a horizontal isothermal circular cylinder, *Int. J. Heat Mass Transf.*, **23**, 971–979 (1980)
2 Farouk, B. and Güçeri, S. I. Natural convection from a horizontal cylinder–laminar regime, *J. Heat Transf.*, **103**, 522–527 (1981)
3 Sparrow, E. M. and Niethammer, J. E. Effect of vertical separation distance and cylinder-to-cylinder temperature imbalance on natural convection for a pair of horizontal cylinders, *J. Heat Transf.*, **103**, 638–644 (1981)
4 Park, S. K. and Chang, K. S. Numerical study on interactive laminar natural convection from a pair of vertically separated horizontal cylinders, *Num. Heat Transf.*, **14**, 61–74 (1988)
5 Farouk, B. and Güçeri, S. I. Natural and mixed convection heat transfer around a horizontal cylinder within confining walls, *Num. Heat Transf.*, **5**, 329–341 (1982)
6 Tokura, I., Saito, H., Kishinami, K. and Muramoto, K. An experimental study of free convection heat transfer from a horizontal cylinder in a vertical array set in free space between parallel walls, *J. Heat Transf.*, **105**, 102–107 (1993)
7 Sparrow, E. M. and Pfeil, D. R. Enhancement of natural convection heat transfer from a horizontal cylinder due to vertical shrouding surfaces, *J. Heat Transf.*, **106**, 124–130 (1984)

8 Lacroix, M. Natural convection heat transfer around two heated horizontal cylinders inside a rectangular cavity cooled from above, *Num. Heat Transfer* (*A*), **21**, 37–54 (1992)
9 Lacroix, M. Analysis of natural convection heat transfer between two horizontal cylinders and their enclosure, *Trans. Canad. Soc. Mech. Eng.*, **16**, 17–32 (1992)
10 Kim, D. M. and Viskanta, R. Effect of wall heat conduction on natural convection heat transfer in a square enclosure, *J. Heat Transf.*, **107**, 139–146 (1985)
11 Du, Z. G. and Bilgen, E. Coupling of wall conduction with natural convection in a rectangular enclosure, *Int. J. Heat Mass Transf.*, **35**, 1969–1975 (1992)
12 Lacroix, M. and Garon, A. Numerical solution of phase change problems: an Eulerian–Lagrangian approach, *Num. Heat Transf.* (*B*), **21**, 57–78 (1992)
13 Patankar, S. *Numerical Heat Transfer and Fluid Flow*, Hemisphere, Washington, DC (1980)